Applied Thermal Engineering 255 (2024) 124022

Contents lists available at ScienceDirect

Applied Thermal Engineering

journal homepage: www.elsevier.com/locate/apthermeng

Research Paper

# Energy transfer and conversion in the Allam cycle with a multi-stream heat exchanger

Qinghe Guo, Zheng Wang, Yafei Liu, Yi Wu, Zhangquan Wen, Haoran Xu, Peiwang Zhu, Jinsong Zhou *, Gang Xiao *

*Key Laboratory of Clean Energy and Carbon Neutrality of Zhejiang Province, Zhejiang University, Hangzhou 310027, China*
*State Key Laboratory of Clean Energy Utilization, Zhejiang University, 38 Zheda Road, Hangzhou 310027, China*

A R T I C L E I N F O

*Keywords:*
Allam cycle
Supercritical $CO_2$
Oxy-fuel combustion
Thermodynamic analysis
Carbon capture

A B S T R A C T

The Allam cycle is renowned for its high efficiency and low emissions in power generation, utilizing supercritical carbon dioxide as the working fluid. The regenerator, one of the key heat exchangers, plays a crucial role in the system. However, modeling the regenerator is challenging due to the presence of multiple pinch points. This study proposes a regenerator model that employs three multi-stream heat exchanger modules in Aspen Plus. A thermodynamic and economic analysis of the system was conducted and compared with a conventional system utilizing the two multi-stream heat exchanger modules. Simulation results show that the combustion chamber has the highest exergy loss in the system, accounting for 46.9 % of the total exergy loss. The turbine is identified as the most capital-intensive component, representing 44.9 % of the total equipment investment. Furthermore, a sensitivity analysis was conducted on key parameters. The results indicate that under certain operating conditions, the heat provided by the air separation unit is insufficient to reduce the temperature difference at the hot outlet of the regenerator. Compared to the conventional Allam cycle system using the 2R model, the 2R model predicts deviations of up to 28.9 %. This proposed model provides a new approach for the efficient allocation of energy utilization in the multi-stream heat exchange process within the Allam cycle system.

## 1. Introduction

In recent years, global warming has become more severe [1], highlighting the urgent need to reduce greenhouse gas emissions [2]. The power industry is a significant source of global carbon dioxide ($CO_2$) emissions [3], particularly from conventional coal and gas-fired power plants. To address this issue, a variety of technologies have been developed and implemented, including carbon capture, utilization, and storage (CCUS) [4], renewable energy integration [5–8], and advanced energy efficiency measures [9–12]. However, integrating $CO_2$ capture technologies with conventional power plants can increase costs and reduce efficiency by 10 % or more [13]. Therefore, it is crucial to develop novel, highly efficient, and cost-effective carbon capture technologies.

Oxy-fuel combustion technology is recognized as a promising solution for reducing $CO_2$ emissions from fossil fuel-fired power plants [14]. Compared to the other carbon capture technologies, it is noted for its cost-effectiveness. Several power cycles based on oxy-fuel combustion have been proposed, including the Graz cycle [15], the MATIANT cycle [16], SCOC-CC [17] (Semi-Closed Oxy-Combustion Combined Cycle), CES cycle [18], and the Allam cycle [19]. The International Energy Agency (IEA) [20] has evaluated these oxy-fuel combustion power cycles. Under conditions of a turbine inlet temperature of 1150 °C, and a turbine inlet pressure of 30 MPa, the Allam cycle demonstrates the highest efficiency (55.1 %) and superior economic performance.

The Allam cycle, a semi-closed Brayton cycle, was originally developed by Allam et al. [19]. This cycle employs $CO_2$ as the working fluid, potentially enabling 100 % carbon capture without additional carbon capture equipment. Using carbon dioxide as a working fluid for power generation offers several advantages, including high efficiency, flexibility, and system compactness. It can be combined with various heat sources, such as solar energy, nuclear energy, and geothermal energy, to further improve overall system efficiency [21,22]. Scaccabarozzi et al. [23] conducted a thermodynamic analysis and optimization of the Allam cycle, revealing that its optimal efficiency could reach 54.80 %. Zhu et al. [24] introduced modifications to the Allam cycle, proposing the Allam-Z cycle. These modifications involve reducing the turbine

* Corresponding authors at: Key Laboratory of Clean Energy and Carbon Neutrality of Zhejiang Province, Zhejiang University, Hangzhou 310027, China.
*E-mail addresses:* zhoujs@zju.edu.cn (J. Zhou), xiaogangtianmen@zju.edu.cn (G. Xiao).

https://doi.org/10.1016/j.applthermaleng.2024.124022
Received 9 April 2024; Received in revised form 16 July 2024; Accepted 22 July 2024
Available online 23 July 2024
1359-4311/

**Nomenclature**

*Acronyms*

| | |
|---|---|
| ASU | air separation unit |
| CCUS | carbon capture, utilization, and storage |
| $CO_2$ | carbon dioxide |
| Comb | combustor |
| Comp | compressor |
| Cond | condenser |
| G | generator |
| HX | heat exchanger |
| IEA | International Energy Agency |
| LHV | low heating value |
| NG | natural gas |
| Regen | regenerator |
| Sep | water separator |
| Tur | turbine |
| 2R | two regenerators |
| 3R | three regenerators |

*Symbols*

| | |
|---|---|
| Ex | exergy, kW |
| ex | spefic exergy, kJ / kg |
| h | specific enthalpy, kJ / kg |
| m | mass flow rate, kg/s |
| P | pressure, MPa |
| Q | heat flow, kW |
| s | specific entropy, $kJ \cdot kg^{-1} \cdot K^{-1}$ |
| T | temperature, °C |
| W | power, kW |
| η | efficiency, % |

*Subscripts*

| | |
|---|---|
| in | input |
| mixture | $CO_2$ and oxygen |
| net | net power output |
| out | output |
| o | standard reference state |
| tur | turbine |

inlet temperature and increasing the turbine outlet pressure, eliminating the need for turbine cooling techniques and allowing the replacement of the $CO_2$ compressor with a pump. Dokhaee et al. [25] utilized Thermoflow software to model and analyze the primary components of the Allam cycle. The simulation results indicated that the net efficiency of the cycle could reach 54 % when a three-stage intercooling system was used. Chan et al. [26] proposed a novel Allam cycle incorporating a reheat system. Their analysis highlighted the significant impact of the combustor outlet temperature on cycle performance. Zhao et al. [27] designed an integrated coal gasification Allam cycle, achieving a net efficiency of 38.87 % under a turbine inlet temperature of 1200 °C.

The regenerator in the Allam cycle is a key component for heat recovery. Due to the turbine exhaust temperature often reaching as high as 700 °C, the power of the regenerator is usually several times that of the turbine [28]. Unlike the closed Brayton cycle, the regenerator in the Allam cycle is a multi-stream heat exchanger [29]. The two hot streams are the turbine exhaust and the compressed air from the ASU while the three cold streams are the turbine cooling stream, oxidant stream, and $CO_2$ stream. Compared to a two-stream heat exchanger, a multi-stream heat exchanger offers high efficiency, a more compact structure, and minimal energy loss. Despite its complex design, it is widely used in gas separation and petrochemical industries [30]. The compact internal structure of a multi-stream heat exchanger allows rapid concentration of cold and hot streams, facilitating efficient energy transfer. Additionally, its larger surface area to volume ratio supports large-scale energy transfer. Kindra et al. [31] studied the effect of operating parameters on cycle net efficiency, total size, and overall cost of the heat exchanger. They found that a 1 °C increase in the pinch point within the heat exchanger led to an average decrease of 0.13 % in cycle net efficiency and a 0.28 % increase in fuel costs. Rogalev et al. [32] developed a process diagram and performed thermodynamic analysis on a multi-stream heat exchanger consisting of five two-stream heat exchangers. They recommended using streams with the lowest temperatures to cool the heated streams.

Despite extensive research on the Allam cycle, further clarification is needed regarding energy conversion in the multi-stream heat exchanger. Previous studies typically relied on the first law of thermodynamics for energy accounting and evaluation. However, assessing comprehensive energy utilization in multi-stream energy transfer is challenging due to varying energy grades. Different streams within the multi-stream heat exchanger have varying energy grades and heat capacity, which means that there may be multiple pinch points within the regenerator.

In this study, a novel regenerator model is proposed, which is constructed by connecting three multi-stream heat exchanger modules in series using Aspen Plus software. This model effectively analyzes the energy conversion under multi-stream heat exchange conditions, thereby improving the overall efficiency of the system. The impact of ASU on the system is critically discussed. Additionally, an exergy analysis and an economic analysis of the system were conducted, guiding the commercial development and demonstration of the Allam cycle.

## 2. System description

### 2.1. Allam cycle

The schematic of the Allam cycle is shown in Fig. 1. Gaseous fuel (stream 1) is compressed by the natural gas compressor ($Comp_{NG}$) and mixed with the preheated oxidant stream (stream 22) from the regenerator (Regen) before entering the combustor (Comb). Diffusion combustion, which is more stable and simpler than pre-mixed combustion, is typically used in the combustion chamber [19]. The $CO_2$ stream (stream 21) is fed into the combustor to regulate its outlet temperature, which is 1150 °C. The flue gas, at a pressure of 30 MPa, enters the turbine (Tur) to drive the generator (G). The turbine's outlet pressure is 3 MPa, and its exhaust (stream 4) mainly consists of $CO_2$ and about 5 % water vapor. The turbine exhaust temperature decreases from approximately 730 °C to 43 °C in the Regen. During this process, heat regeneration occurs and the energy released from the condensation of water vapor is recovered [33]. Subsequently, water (stream 7) is separated from the system by the water separator (Sep). High-purity $CO_2$ (stream 6) is compressed to 10 MPa by a $CO_2$ compressor ($Comp_{CO_2}$) and further cooled in a condenser (Cond) to separate high-density $CO_2$ (stream 12). The residual $CO_2$ is then compressed to 30 MPa by a $CO_2$ pump ($Pump_{CO_2}$) and a mixture pump ($Pump_{mixture}$) and enters the cold end of the Regen. A portion of $CO_2$ (stream 13) is mixed with oxygen (stream 15) over 99.5 % purity (molar basis). Since the specific heat capacity of $CO_2$ at low pressure is lower than at high pressure [34], the heat generated from the compression of ASU is added to the Regen to reduce the temperature difference at the hot end [35].

### 2.2. Three-regenerators analytical method

Before modeling the Regen, the initial temperature of each stream must be determined, as it influences the energy grade. In the Allam cycle, there are two hot streams: turbine exhaust and compressed air from ASU. According to the literature [23], a temperature of 265 °C is

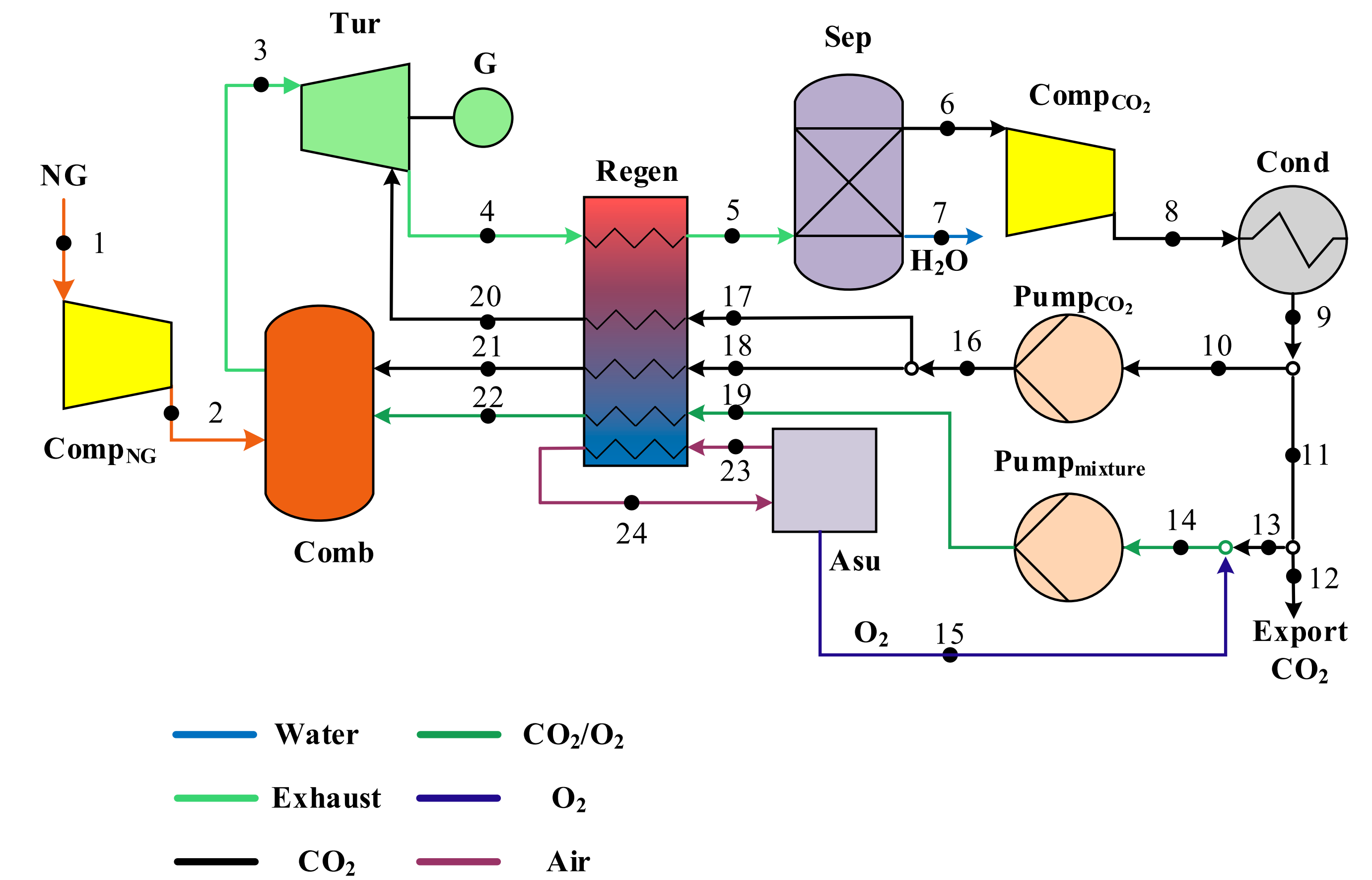


**Fig. 1.** Schematic diagram of Allam cycle.

selected for the compressed air (stream 23) in this work, considering a certain temperature drop. The temperature of turbine cooling stream (stream 20) is not constant [23,33]. In this study, it is set at 400 °C, and the effect on system performance will be discussed in detail in subsequent chapters.

Using the pinch point design method proposed by Linnhoff et al. [36], a temperature-enthalpy diagram for all the streams can be created, as shown in Fig. 2a. It is a systematic approach for heat integration and process optimization. By analyzing the streams within the process, it determines the optimal heat exchanger network design, thereby maximizing energy efficiency, reducing energy consumption, and minimizing costs. By combining all the hot streams and cold streams, two composite

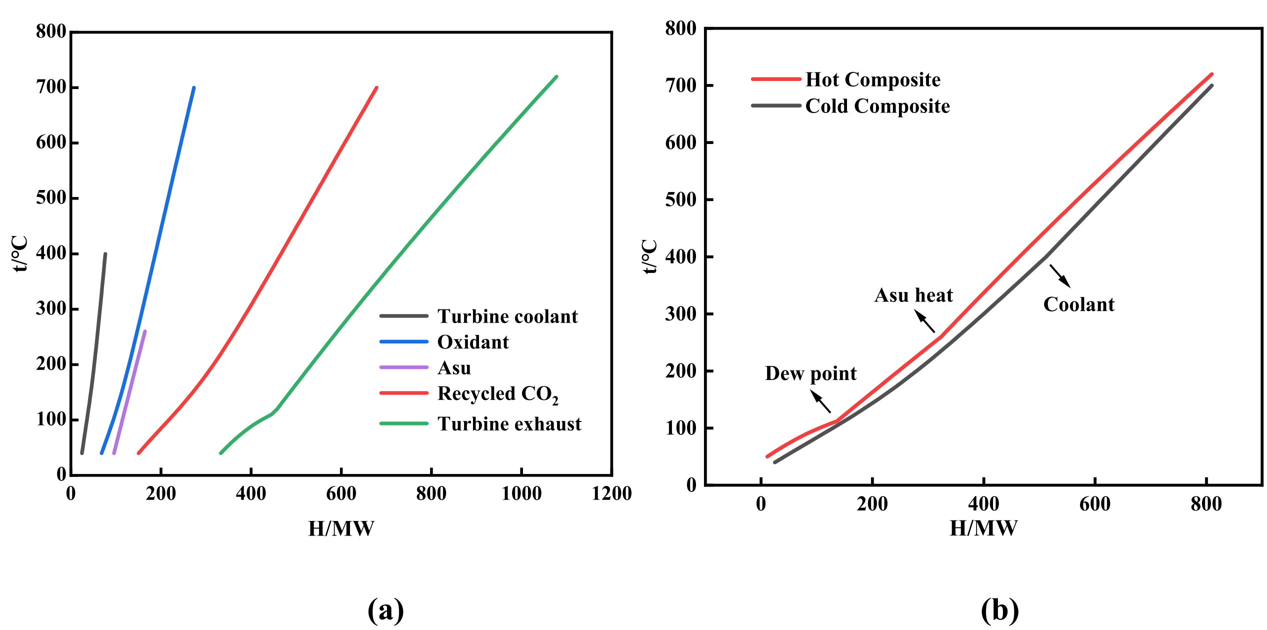


**Fig. 2.** (a) Temperature-enthalpy of streams; (b) Temperature-enthalpy of composite streams.

curves can be obtained: the hot composite curve and the cold composite curve, as shown in Fig. 2b. By horizontally shifting the composite streams, the positions of the minimum temperature difference in the heat transfer process can be identified. Fig. 2b indicates that potential pinch points may occur at the hot end of Regen, where compressed air from the ASU is introduced, and at the dew point where water vapor condensation begins.

To analyze the temperature differences at these specific positions, a new Regen (3R, three regenerators) model was proposed and developed in Aspen Plus. As shown in Fig. 3, it consists of three multi-stream heat exchanger modules. In this model, the multi-stream heat exchangers 1 (HX.1), 2 (HX.2), and 3 (HX.3) handle heat transfer across different temperature ranges: from turbine exhaust temperature to compressed air temperature, from compressed air temperature to water vapor's dew point temperature, and from water vapor's dew point temperature to the cold end temperature of the Regen, respectively. According to the literature [34], the minimum pinch point of the Regen is 5 °C, occurring at the hot inlet of HX.3. The hot outlet temperature of HX.2 is set to the dew point of water vapor, calculated based on the exhaust composition. The hot inlet temperature of HX.2 is 265 °C, corresponding to the temperature of compressed air from the ASU. The temperature difference of the hot outlet of HX.2 and HX.1 should be discussed separately, with the overall goal of minimizing the temperature difference at the hot end of HX.1, while ensuring both remain no less than 20 °C [35]. It is important to note that the hot end temperature difference of HX.3 may not always be 20 °C due to the difference in heat capacity between high-pressure and low-pressure streams. Although the specific heat capacity of the low-pressure stream is lower than that of high-pressure stream, the mass flow rate of the high-pressure stream is lower than that of low-pressure stream. Additionally, the turbine cooling stream only heats up to a lower temperature despite the introduction of an oxidant stream on the high-pressure side. Therefore, the heat capacity on the low-pressure side may not necessarily be lower than that on the high-pressure side. If the hot end temperature difference of HX.2 remains at 20 °C and the hot end temperature difference of HX.1 cannot be reduced to 20 °C, it indicates that the heat provided by the turbine exhaust is insufficient to heat the recirculating stream to a temperature of 20 °C lower than the exhaust temperature. If the temperature difference at the hot end of HX.1 is less than 20 °C, there must be an excess of heat from the compressed air. In this case, the mass flow rate of the compressed air may need to be reduced to achieve a temperature difference of 20 °C at the hot end of HX.1. Consequently, the temperature difference at the hot end of HX.2 will be higher than 20 °C.

This model ensures that the cold streams do not transfer heat to the hot streams during the energy transfer process and clearly differentiates the energy transfer conditions in different temperature ranges.

## 3. Models and assumptions

Previous research [37] indicates that Aspen Plus is widely used as a modeling and analysis tool. It is a process simulation software that offers numerous physical property models and databases. In this study, Aspen Plus Version 11 was utilized to develop and calculate the current model. To perform more complex and comprehensive computational tasks, a connection was established between MATLAB and Aspen Plus using the Aspen Plus COM interface. The thermophysical property parameters for thermodynamic calculations were retrieved from the Reference Fluid Thermodynamic and Transport Properties (REFPROP) database.

### 3.1. Main components model

#### 3.1.1. Combustor

The combustor is simulated using the Rstoic module, which is based on material balance. In this calculation, a molar ratio of 1:2 between oxygen and methane is assumed, with $CO_2$ and $H_2O$ as the combustion products. Factors such as heat dissipation, incomplete combustion, and the dissociation of combustion products are neglected. The Peng-Robinson equation of state [38] is utilized for calculations. The desired outlet temperature of the combustor is specified by adjusting the mass flow rate of $CO_2$ (stream 21) using the 'Design Specification' feature in Aspen Plus.

#### 3.1.2. Turbine cooling model

In the Allam Cycle, the outlet temperature of the combustor often exceeds the allowable temperature of turbine blades made of existing materials[39]. In this study, the maximum allowable temperature for turbine blades was selected to be 860 °C. To address this issue and ensure proper turbine operation, an improved continuous expansion model proposed by Scaccabarozzi et al. [23] was adopted. This model is based on El-Masri's continuous expansion model which divided the expansion process into N+1 stages. Each step consisted of a turbine expansion and a pressure drop module. In the first N turbine stages, the mainstream temperature remains above 860 °C. After expansion in the turbine, the mainstream is mixed with the cooling stream by a mixer. It is assumed that the expansion ratio remains constant for the first N turbine stages. In the last turbine stage, the inlet temperature is equal to 860 °C, and cooling is no longer required. The calculation process accounts for the pressure loss caused by each mixing of the cooling stream and mainstream, using specific calculation formulas and relevant coefficients provided in reference [23]. To ensure computational precision and optimize computing resources, N is set to 15 [27]. In Aspen Plus, the Compr module, Mixer module, and Valve module are used to implement this process. The calculation process involves adjusting the expansion ratios of the preceding N turbine stages to achieve an inlet temperature of 860 °C for the N+1 turbine stage. The calculation starts by assuming the expansion ratios for the first N stages and obtaining the turbine outlet temperature and the temperatures of the circulating $CO_2$ streams. Then, the expansion ratios for the preceding N stages are iteratively adjusted based on the calculated temperature values until the desired conditions are achieved.

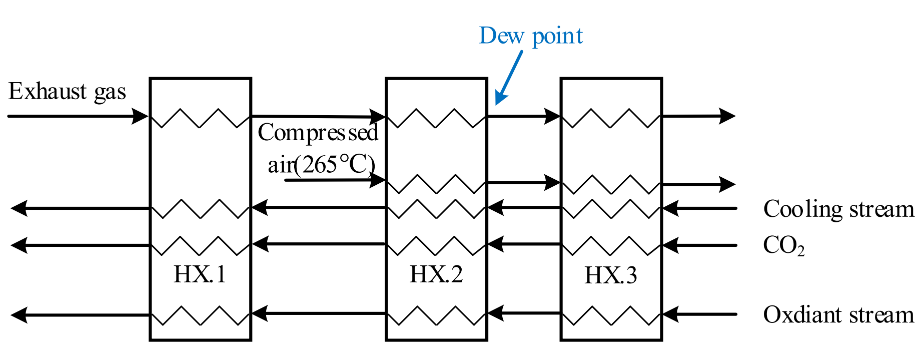


**Fig. 3.** Schematic diagram of multi-stream heat exchanger.

### 3.1.3. ASU model

The ASU is essential for supplying high-purity oxygen and heat of compression to the Regen. While many industrial processes use multi-stage compression and intercooling between stages [40] to reduce the power consumption of compressors, Allam et al. [29] found that single-stage compression in the ASU does not reduce the overall cycle efficiency of the Allam cycle.

In the ASU, oxygen is usually supplied at concentrations of either 95 % or 99.5 %. Research by Hume et al. [41,42] shows that using 95 % oxygen increases energy consumption in the compression process and does not meet the required concentration of captured $CO_2$, thus increasing the cost of subsequent purification units. In this study, the ASU is not modeled separately; instead, the model developed by Beysel et al. [43] is used. For simplicity, it is assumed that the liquid oxygen from the ASU is free of impurity gases.

## 3.2. Exergy model

The first law of thermodynamics elucidates the conservation of energy from a quantitative perspective, but the quality levels of different forms of energy are not the same. During energy conversion, the quality tends to degrade. The efficiency of conversion depends on environmental conditions and the degree of irreversibility in the process. To evaluate the irreversibility of thermodynamic processes, the main components of the system are analyzed based on the second law of thermodynamic[26,44].

Exergy destruction can be determined using the following equation:

$$Ex_d = Ex_i - Ex_o + Ex_{work} \tag{1}$$

where, $Ex_i$ (kW) and $Ex_o$ (kW) are the inlet and outlet exergy of the working fluid.

For the working fluid, its exergy can be calculated by [45]:

$$Ex = m\cdot(ex^{ph} - ex^{ch}) \tag{2}$$

The physical specific exergy can be determined through its specific enthalpy (h, kJ/kg) and specific entropy(s, kJ·kg$^{-1}$ K$^{-1}$):

$$ex^{ph} = h - h_0 - T_0\cdot(s\text{-}s_0) \tag{3}$$

where the reference environment is chosen as 298.15 K and 1.013 bar.

The chemical specific exergy is determined using the calculation methods found in the literature [46]:

$$ex^{ch} = 1.04\cdot LHV_{NG} \tag{4}$$

where, $LHV_{NG}$ denotes the low heating value of natural gas, kJ/kg.

## 3.3. Economic model

Economic analysis of each component's cost share aids in understanding cost distribution, thereby enabling targeted cost reduction strategies and improved resource allocation. Analyzing cost shares can also reveal inefficiencies within the system. High-cost components can be optimized or redesigned to enhance overall system efficiency. The investment cost of the Allam cycle is calculated based on information reported in the literature [47–49].

## 3.4. Thermodynamic model

The mathematical models of the main components are shown in Table 1. It is worth noting that these equations are derived based on the first law of thermodynamics. When performing thermodynamic calculations for the regenerator, the second law of thermodynamics also needs to be considered.

This article introduces system efficiency ($\eta$) to evaluate cycle performance. $\eta$ is the ratio of the net power output to the heating value of the fuel input, represented by:

$$\eta = \frac{W_{net}}{Q_{NG}} \tag{5}$$

where, $W_{net}$ represents the net power output of the system and $Q_{NG}$ refers to the heating value of the fuel input, kW.

Additionally, $W_{net}$ can be further expressed as:

$$W_{net} = W_{tur}\text{-}W_{NG}\text{-}W_{comp}\text{-}W_{pump}\text{-}W_{ASU} \tag{6}$$

Similarly, $Q_{NG}$ can be further expressed using the equation:

$$Q_{NG} = m_{NG}\cdot LHV_{NG} \tag{7}$$

where, $m_{NG}$ represents the mass flow rate of natural gas and $LHV_{NG}$ denotes the low heating value of natural gas.

To analyze the effect of ASU on the system, W is defined as the power output excluding the power consumption of ASU.

$$W = W_{tur}\text{-}W_{NG}\text{-}W_{comp}\text{-}W_{pump} \tag{8}$$

**Table 1**
Mathematical model of the main components.

| Components | Mathematical model |
|---|---|
| Comb | $m_3 = m_2 + m_{21} + m_{22}$ <br> $m_3h_3 = m_2h_2 + m_{21}h_{21} + m_{22}h_{22}$ |
| Tur | $m_4 = m_3 + \sum_{i=1}^{N} m_{Ci}$ <br> $W_{tur} = (m_3 + m_{C1})(h_{in}\text{-}h_{out}) + \sum_{i=2}^{N+1} m_{Ci}\,(h_{in}\text{-}h_{out})$ |
| Regen | $m_4(h_4\text{-}h_5) = m_{17}(h_{20}\text{-}h_{17}) + m_{18}(h_{21}\text{-}h_{18}) + m_{19}(h_{22}\text{-}h_{19}) + Q_{ASU}$ |
| Cond | $m_{hot}(h_{hot,in}\text{-}h_{hot,out}) = m_{cold}(h_{cold,out}\text{-}h_{cold,in})$ |
| Comp | $W_{comp} = m(h_{out}\text{-}h_{in}) = m(h_{outs}\text{-}h_{in})/\eta_{comp}$ |
| Pump | $W_{pump} = m(h_{out}\text{-}h_{in}) = m(h_{outs}\text{-}h_{in})/\eta_{pump}$ |

Note: $m_{Ci}$ refers to the mass flow rate of the i-th stage cooling flow.

## 3.5. Basic assumption and model validation

To simplify the calculations and account for the features of Aspen Plus software, the following assumptions are made for this simulation:

(1) The system reaches a steady-state condition, neglecting kinetic and potential energy, as well as heat transfer with surroundings.
(2) Pressure drops and efficiency of the main components are shown in Table 2 based on literature values [50], and the separation efficiency of Sep is assumed to be 100 %.
(3) Both the compressors and turbines are assumed to have constant isentropic efficiencies, with the efficiencies of turbomachines provided in Table 2.
(4) The natural gas composition is assumed to be methane with an initial pressure of 3 MPa and an initial temperature of 15 °C [26].

The calculations are performed using the relevant parameters suggested by Allam et al.[29], with the main parameters listed in Table 3.

**Table 2**
Design parameters of Allam cycle.

| Items | Unit | Value |
|---|---|---|
| Pressure drops of HX.1(high-pressure side) | % | 1 |
| Pressure drops of HX.1(low-pressure side) | % | 3 |
| Pressure drops of Comb | % | 1 |
| Pressure drops of Sep | % | 2 |
| Isentropic efficiency of Tur | % | 90 |
| Isentropic efficiency of $Comp_{CO_2}$ | % | 85 |
| Isentropic efficiency of $Comp_{NG}$ | % | 90 |
| Mechanical efficiency of Compressors | % | 99 |
| Isentropic efficiency of pumps | % | 85 |
| Mechanical efficiency of pumps | % | 98 |

**Table 3**
Boundary conditions of the cycle.

| Parameters | Value | Unit |
|---|---|---|
| $m_1$ | 10 | kg/s |
| $T_3$ | 1150 | °C |
| $P_3$ | 30 | MPa |
| $P_4$ | 3 | MPa |
| $T_6$ | 17 | °C |
| $P_9$ | 10 | MPa |
| $T_{20}$ | 400 | °C |
| $T_{23}$ | 265 | °C |

**Table 4**
Model validation of the regenerator.

| Items | Ref. [32] | This work | Error (%) |
|---|---|---|---|
| $T_5$(°C) | 74.0 | 73.0 | −1.3 |
| $T_{20}$(°C) | 200.0 | 200.0 | 0.0 |
| $T_{21}$(°C) | 653.0 | 650.1 | −0.4 |
| $T_{22}$(°C) | 653.0 | 650.1 | −0.4 |
| $T_{24}$(°C) | 100.0 | 100.0 | 0.0 |
| Power of regenerator (MW) | 524.0 | 526.9 | 0.5 |

The calculation process is illustrated in Fig. 4.

To validate the accuracy of the model, the simulation results were compared with the published literature[32]. The parameters of the streams were aligned with those in the literature. The results are presented in Table 4 which demonstrates that the relative errors fall within an acceptable range, suggesting that the model predicts the performance of the regenerator effectively.

## 4. Results and discussion

This chapter comprehensively discusses the system performance of the Allam cycle. Initially, it analyzes the exergy loss and economic performance under basic design conditions. Subsequently, a parameter analysis is conducted to evaluate the impact of key parameters on system performance, followed by a comparative analysis with the multi-stream heat exchanger mentioned in the literature.

### 4.1. Exergy analysis

Fig. 5 shows the exergy destruction proportions of various components under basic design conditions, with the combustor and turbine being the primary sources of exergy destruction, accounting for 46.9 % and 24.8 %, respectively. This indicates that the combustor and turbine are critical areas for improving system efficiency.

To address the high exergy destruction in the combustor, increasing the combustion temperature can help. However, the maximum temperature tolerance of Regen's hot-end materials limits this approach. Therefore, while raising the combustion temperature, it is also necessary to increase the pressure in the combustor. This will enhance the expansion effect of the working fluid and reduce the turbine outlet temperature.

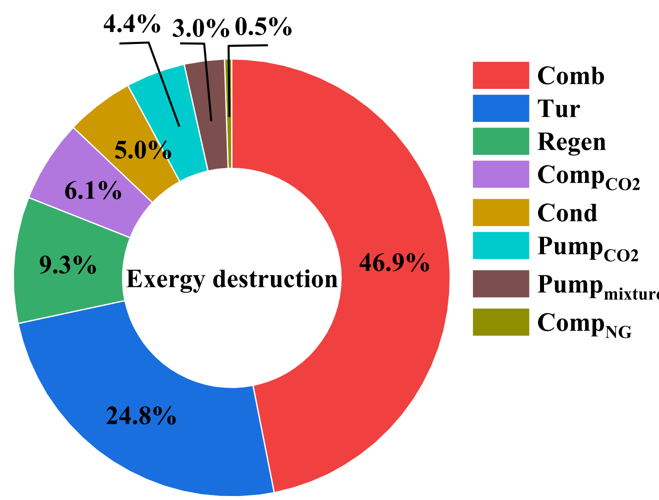


**Fig. 5.** The distribution of exergy destruction.

### 4.2. Economic analysis

Fig. 6 shows the proportion of equipment costs in the total equipment costs under basic design conditions. The turbine and compressor dominate the equipment investment costs, accounting for 44.9 % and

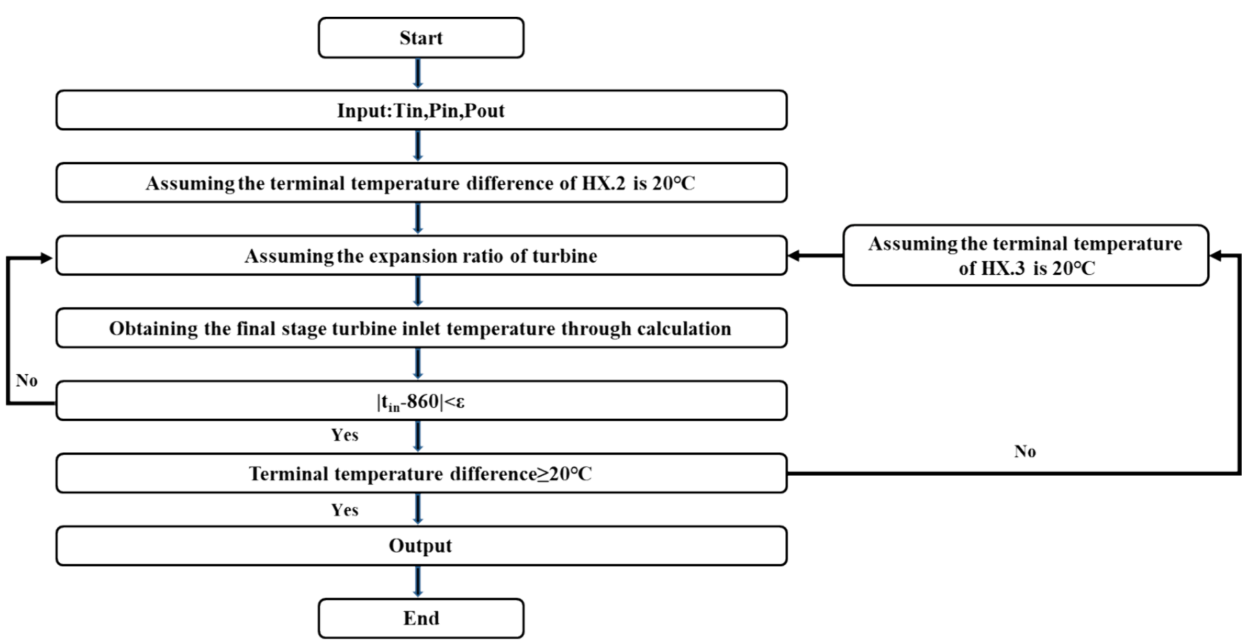


**Fig. 4.** Algorithm for the design calculation of the cycle.

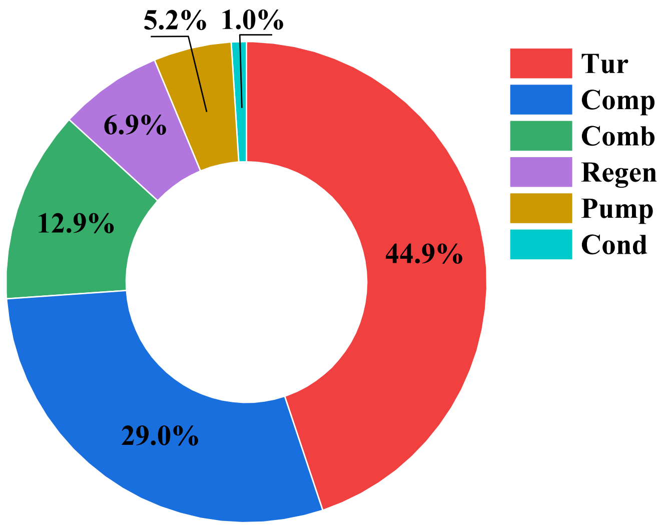


**Fig. 6.** The distribution of equipment investment cost.

29.0 %, which indicates their crucial roles. Improving their efficiency and reliability is essential for enhancing system performance and reducing overall costs. To optimize the economic performance of the Allam cycle, it is recommended to invest in high-efficiency turbines and compressors to lower energy consumption. Simplifying the design and maintenance of regenerators and combustors can help reduce costs.

### *4.3. Sensitivity analysis*

#### *4.3.1. Sensitivity of turbine inlet pressure*

Fig. 7a shows the effect of turbine inlet pressure ($P_{tur,in}$) and temperature ($T_{tur,in}$) on power (W). Some data points are not plotted because excessively high $T_{tur,in}$ or excessively low $P_{tur,in}$ would result in turbine outlet temperatures ($T_{tur,out}$) exceeding the allowable endurance limits of the materials available [19]. For each $T_{tur,in}$, there is a specific pressure where W reaches its maximum value. As the $T_{tur,in}$ rises, the pressure corresponding to the maximum W also increases. At a $P_{tur,in}$ of 30 MPa and a $T_{tur,in}$ of 1150 °C, W reaches its peak. This is because, with higher turbine temperatures, the carbon dioxide flow rate to the combustion chamber decreases. These two factors have opposite effects on W, causing it to increase first and then decrease.

Fig. 7b shows the effect of turbine inlet pressure ($P_{tur,in}$) and temperature ($T_{tur,in}$) on system efficiency ($\eta$). It can be observed that when considering the penalty effect of the ASU, $\eta$ shows a different trend compared to Fig. 7a. As $P_{tur,in}$ increases from 20 MPa to 26 MPa, $\eta$ significantly improves. However, further increasing $P_{tur,in}$ to 40 MPa results in only minor changes in $\eta$. This is because higher $P_{tur,in}$ leads to a lower turbine outlet temperature ($T_{tur,out}$), reducing the $CO_2$ flow rate used to regulate the combustion chamber temperature. Consequently, both turbine power output and compressor power consumption decrease. Additionally, the compression heat from the ASU also decreases. Despite the reduction in turbine power output, the decrease in compression heat from the ASU outweighs this effect, leading to an overall increase in net power ($W_{net}$) and $\eta$. As $P_{tur,in}$ increases further, as shown in Fig. 7c, the temperature difference at the hot end of HX.1 increases, causing a rapid reduction in turbine power output. Therefore, $\eta$ shows only minor changes.

Fig. 7d compares the results of the 3R model and the 2R model. The 2R model shows significant deviations in predicting cycle efficiency at lower turbine inlet temperature ($T_{tur,in}$). At 950 °C and 40 MPa, the deviation reaches −16.3 %. When the temperature difference on the hot end of the Regen is small, both models give consistent predictions. The compression heat from the ASU can reduce the temperature difference, but its heat quality is low. At lower $T_{tur,in}$, the temperature difference at the hot end of HX.1 is larger. The 2R model introduces excessive compressed air to reduce this temperature difference. However, when water vapor condenses, it releases a large amount of latent heat. This causes inefficient heat utilization in this temperature range, lowering the system efficiency.

#### *4.3.2. Sensitivity of turbine outlet pressure*

Fig. 8a shows the effect of turbine outlet pressure ($P_{tur,out}$) and temperature ($T_{tur,in}$) on power (W). As $P_{tur,out}$ increases, W also increases. This is because the $CO_2$ pressure is closer to the critical pressure, reducing the compression factor and significantly decreasing the $CO_2$ compression work. Additionally, we observe that W does not increase linearly with the $T_{tur,in}$ at the same $P_{tur,out}$. In the $P_{tur,out}$ range of 2.0–3.5 MPa, W is the highest at a $T_{tur,in}$ of 1150 °C. This is because, with higher $T_{tur,in}$, the $CO_2$ flow rate to the combustion chamber decreases.

Fig. 8b shows that system efficiency ($\eta$) increases monotonically with higher turbine outlet pressure ($P_{tur,out}$) and temperature ($T_{tur,in}$). In addition to power (W) and compression work ($W_{comp}$), the impact of the ASU on the system is also considered. Although W is not the highest at all $P_{tur,out}$ at high $T_{tur,in}$ such as 1350 °C, the required compressed air significantly decreases at high turbine outlet temperature ($T_{tur,out}$). With less compressed air needed, the temperature difference in the Regen can be reduced to 20 °C. When $T_{tur,in}$ is below 1100 °C, despite the additional heat from ASU, the hot end temperature difference of HX.1 remains higher than 20 °C. This implies that a further reduction in the temperature difference at the hot end of HX.1 necessitates a heat source with a higher temperature.

Fig. 8d compares the results of the 3R model and the 2R model. Changes in turbine outlet pressure ($P_{tur,out}$) cause greater calculation deviations in the 2R model compared to changes in turbine inlet pressure ($P_{tur,in}$). This is because, when the temperature difference on the hot side of HX.1 exceeds 20 °C, there is a significant difference in the calculated compressed air demand between the two models. The 2R model calculates a higher compressed air demand than the 3R model, resulting in a lower calculated system efficiency. However, when the temperature difference in the HX.1 is 20 °C, the results from both models are approximately the same.

#### *4.3.3. Sensitivity to turbine coolant temperature*

The effect of turbine cooling temperature ($T_{tur,cool}$) on system efficiency ($\eta$) in the baseline conditions is presented in Fig. 9a. When $T_{tur,cool}$ is lower than 245 °C, the turbine cooling stream no longer enters HX.1 after leaving the hot end of HX.2. It splits into N streams to cool the turbine blades. From Fig. 9a, it can be seen that increasing $T_{tur,cool}$ leads to a decrease in $\eta$. As $T_{tur,cool}$ increases, the flow rate of the cooling stream also increases to achieve the same cooling effect, increasing in net power ($W_{net}$). This is because that higher $T_{tur,cool}$ requires more mass flow to remove the same amount of heat, thereby increasing the overall flow through the turbine and enhancing its power output. However, when $T_{tur,cool}$ exceeds 400 °C, more heat is transferred to the turbine cooling stream in HX.1, causing the temperature difference at the hot end to gradually exceed 20 °C, as shown in Fig. 9b. This increased temperature difference indicates that the regenerator is less effective at transferring heat, leading to a less efficient heat recovery process. Additionally, $W_{net}$ steadily decreases due to the penalty effect of the ASU. This penalty effect underscores the importance of optimizing the integration of the ASU with the overall system to minimize its impact on performance. Power (W) reaches its peak when the turbine cooling stream reaches 400 °C, as shown in Fig. 9c. In other words, a turbine cooling temperature of 400 °C yields the highest cycle efficiency if there is an alternative industrial heat source for reheat. Fig. 9d compares the results of the 3R and 2R models under varying $T_{tur,cool}$. As $T_{tur,cool}$ increases, the 2R model predicts lower efficiency compared to the 3R model. This is due to the increasing HX.1 temperature difference, which results in a higher compressed air flow rate in the 2R model, leading to lower calculated efficiency.

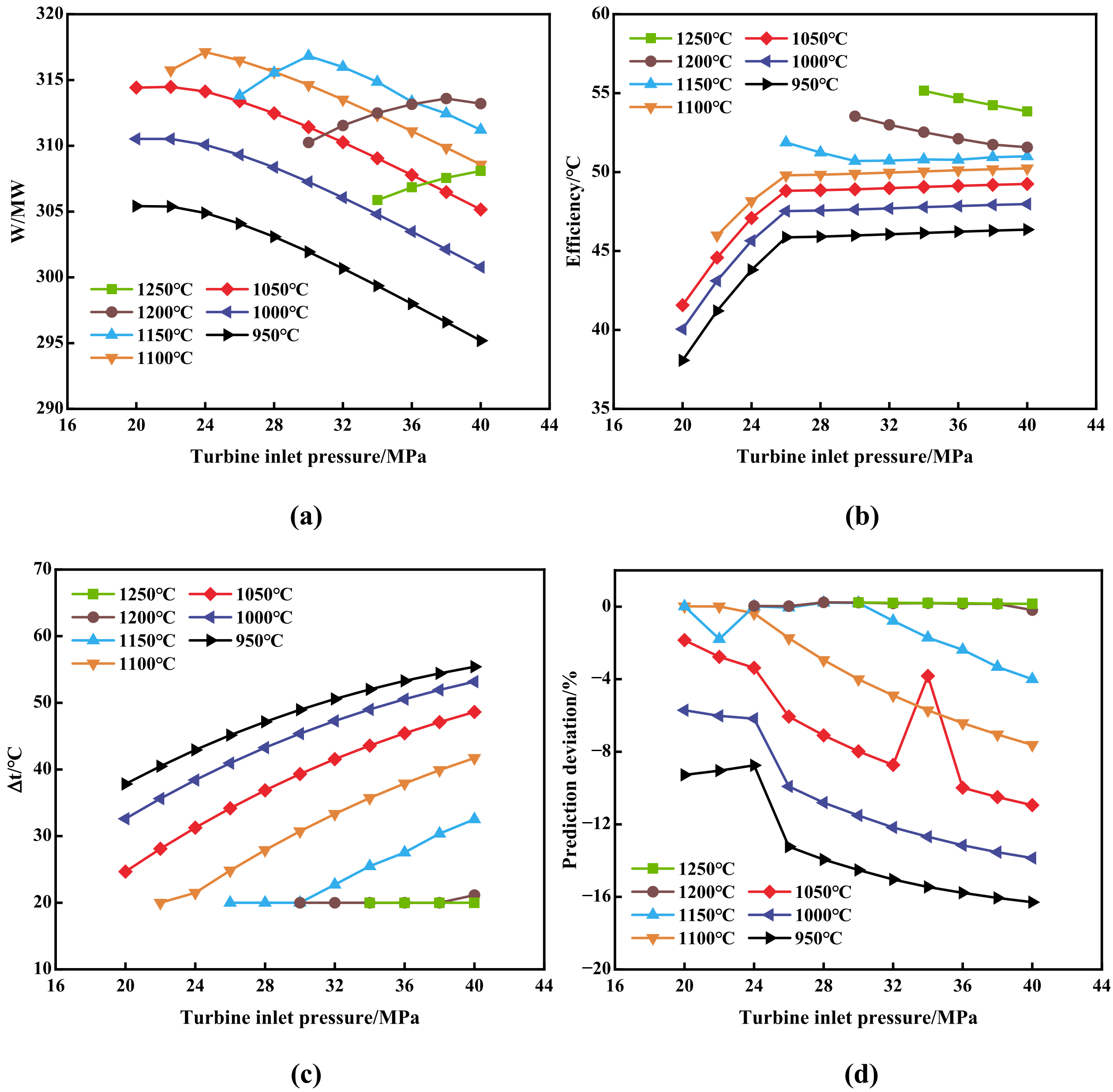


**Fig. 7.** Sensitivity analysis of turbine inlet pressure. (a) power output excluding the power consumption of ASU; (b) system efficiency; (c) temperature difference at the hot end of HX.1; (d) comparison with the 2R model.

#### 4.3.4. *Sensitivity to turbine inlet temperature*

Fig. 10a and Fig. 10b show the variation of power (W) with turbine inlet temperature ($T_{tur,in}$) for different inlet pressure ($P_{tur,in}$) and outlet pressure ($P_{tur,out}$). From Fig. 10a, it can be seen that as $T_{tur,in}$ increases, W initially exhibits an increasing trend, followed by a subsequent decrease. As $T_{tur,in}$ rises, W increases due to the higher thermal energy available for conversion into mechanical work. Simultaneously, the flow rate of the $CO_2$ stream (stream 18), which is used to adjust the combustion temperature, decreases. This reduction in $CO_2$ flow rate leads to a decrease in the compression work ($W_{comp}$) within the system, particularly in components such as the $CO_2$ compressor ($Comp_{CO_2}$) and the mixture pump ($Pump_{mixture}$). Consequently, W exhibits an increasing trend with $T_{tur,in}$ rising. However, with further increases in both $P_{tur,in}$ and $T_{tur,in}$, the negative impact of the reduced $CO_2$ flow rate on W begins to outweigh the positive effect of the increased $T_{tur,in}$. This results in W reaching a maximum value at a certain $T_{tur,in}$. Beyond this optimal temperature, W starts to decrease with further increases in $T_{tur,in}$. This indicates that in the Allam cycle system, a higher $T_{tur,in}$ does not necessarily correlate with a higher net power ($W_{net}$). It is intricately linked to the flow rate of $CO_2$ within the system, highlighting the importance of optimizing both temperature and flow rate for maximum efficiency.

Fig. 10b presents the effect of varying turbine outlet pressure ($P_{tur,out}$) on power (W). Similar to the observations in Fig. 10a, an increase in turbine inlet temperature ($T_{tur,in}$) initially leads to an increase in W, followed by a decrease after reaching a peak value. The peak value of W shifts towards higher $T_{tur,in}$ with increasing $P_{tur,out}$. This shift is attributed to the enhanced ability of the turbine to utilize higher inlet temperatures more effectively at elevated outlet pressures, thereby improving overall power output. However, beyond a certain $T_{tur,in}$, the diminishing returns due to reduced $CO_2$ flow rate and increased thermal losses result in a decline in W.

## 5. Conclusion

In summary, the energy conversion and matching issues of multi-

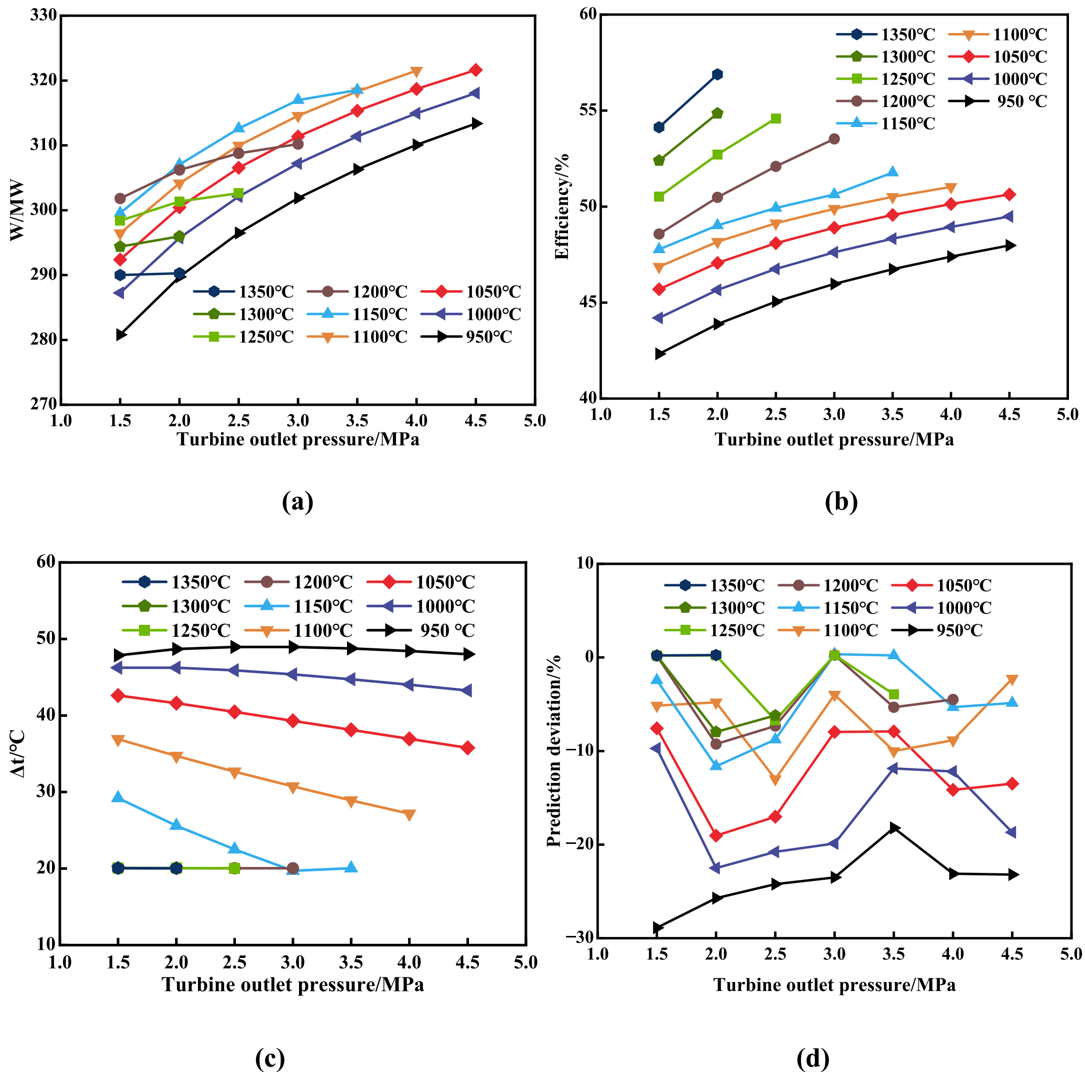


**Fig. 8.** Sensitivity analysis of turbine outlet pressure. (a) power output excluding the power consumption of ASU; (b) system efficiency; (c) temperature difference at the hot end of HX.1; (d) comparison with the 2R model.

stream heat exchangers are studied in the Allam cycle, specifically focusing on the effect of compressed air reheat in ASU. The main conclusions are as follows:

(1) Exergy analysis indicates that the combustion chamber and turbine are the largest sources of exergy loss in the cycle, accounting for 73.7 % of the total losses. Economic analysis points out that the turbine and compressor are the two main components with the highest investment costs, together comprising 73.9 % of the total equipment investment.
(2) Compared to the traditional Allam cycle system using the 2R model, the 2R system shows significant prediction deviations when there is a large temperature difference on the hot side of the recuperator. Under the operating conditions calculated in this study, the maximum deviation can reach 28.9 %.
(3) Sensitivity analysis of key parameters indicates that the penalty effect of compressed air has a significant impact on system efficiency. Increasing the turbine outlet pressure results in a higher turbine outlet temperature, which allows more effective utilization of heat in the high-temperature region. When the turbine outlet temperature is relatively low, relying solely on reheat from the ASU is insufficient to reduce the temperature difference at the hot outlet of the multi-stream heat exchanger to the desired temperature. The introduction of higher-temperature heat sources emerges as a viable solution to further reduce the temperature difference at the hot end of the regenerator.

Future work includes the structural design and techno-economic optimization of multi-stream heat exchangers to reveal their impact on the system's techno-economic performance. This primarily involves analyzing the fluid dynamics characteristics within the multi-stream heat exchanger, including flow resistance, pressure drop, and fluid distribution, to optimize the exchanger's design for improved heat exchange efficiency. Additionally, the selection of materials for the multi-stream heat exchanger and their durability and corrosion resistance under high-temperature and high-pressure conditions will be investigated. Experimental tests under actual operating conditions will be conducted to validate the design and performance of the multi-stream heat exchanger. Through iterative design optimization, the system performance of the Allam cycle will be enhanced while reducing capital investment costs.

## Declaration of competing interest

The authors declare that they have no known competing financial interests or personal relationships that could have appeared to influence

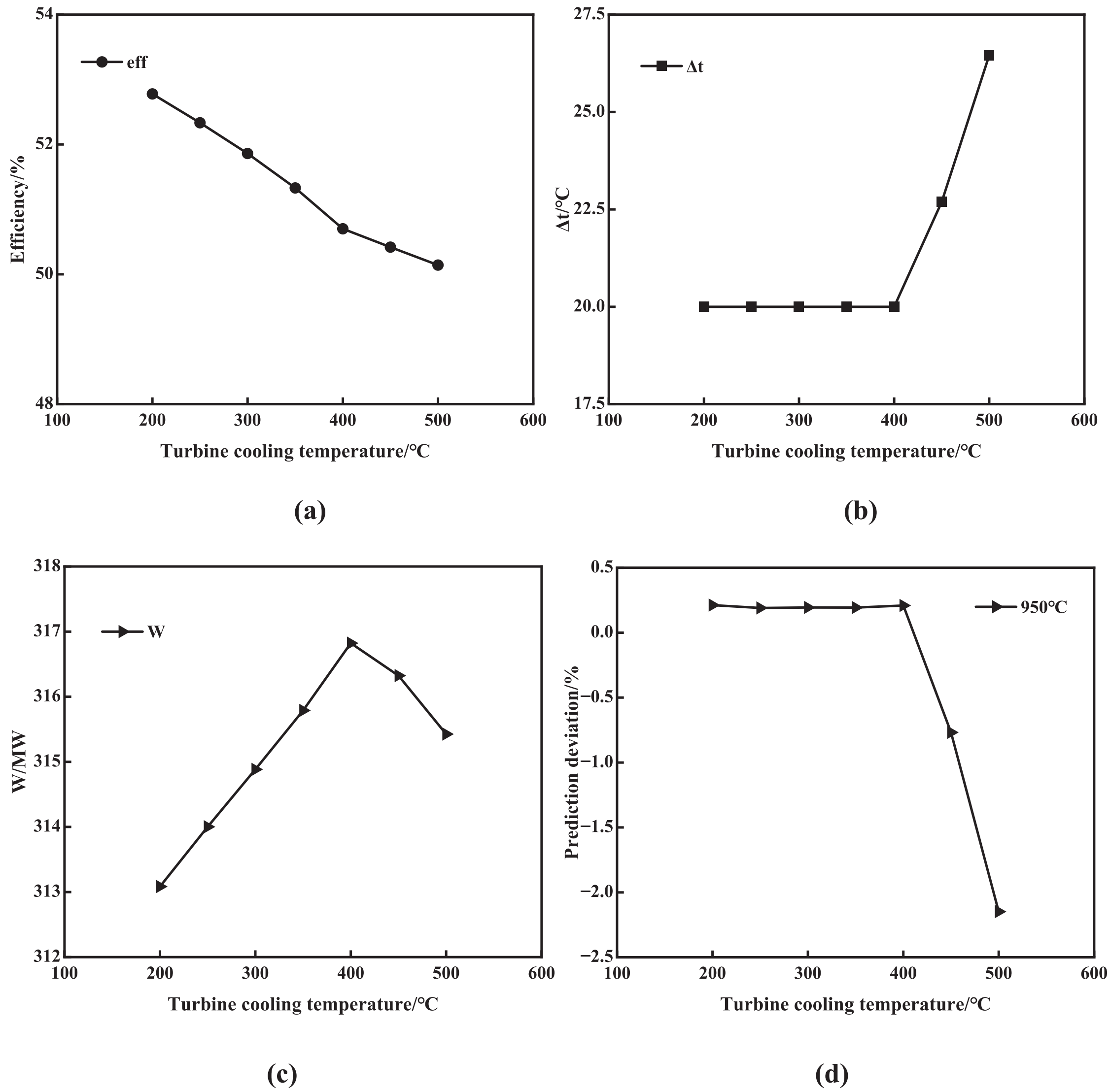


**Fig. 9.** Sensitivity analysis of turbine cooling temperature. (a) system cycle efficiency; (b) temperature difference at the hot end of HX.1; (c) power output excluding the power consumption of ASU; (d) comparison with the 2R model.

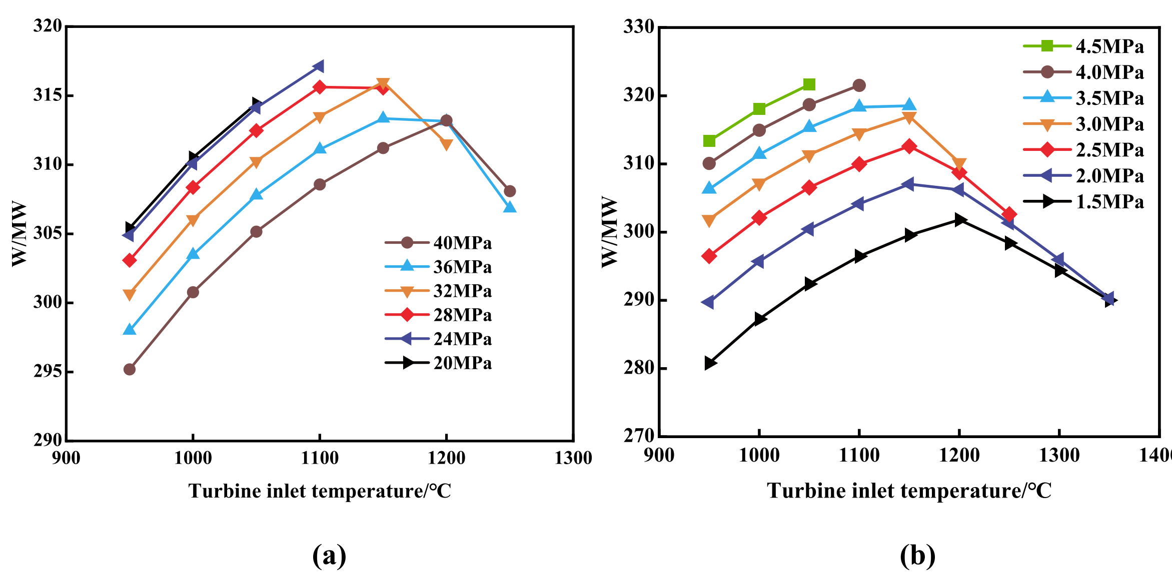


**Fig. 10.** Sensitivity analysis of turbine inlet temperature (a) turbine inlet pressure; (b) turbine outlet pressure.

the work reported in this paper.

## Data availability

Data will be made available on request.

## Acknowledgement

The authors gratefully acknowledge the National Key R&D Program of China (2023YFB4102205), the National Natural Science Foundation of China (52325605), and the Fundamental Research Funds for the Central Universities (2022ZFJH04).

## References

[1] M. Mace, Mitigation commitments under the Paris Agreement and the way forward, Clim. Law 6 (2016) 21–39.
[2] S. Raza, E. Ghasali, M. Raza, C. Chen, B. Li, Y. Orooji, H. Lin, C. Karaman, H. Karimi Maleh, N. Erk, Advances in technology and utilization of natural resources for achieving carbon neutrality and a sustainable solution to neutral environment, Environ. Res. 220 (2023) 115135.
[3] N.A. Manaf, G. Weiss, A. Abbas, Relevancy of Emission Reduction Fund (ERF) policy towards large-scale deployment of carbon capture technology in black coal-fired power plant, J. Clean. Prod. 211 (2019) 1471–1479.
[4] M.J. Regufe, A. Pereira, A.F. Ferreira, A.M. Ribeiro, A.E. Rodrigues, Current developments of carbon capture storage and/or utilization–looking for net-zero emissions defined in the Paris agreement, Energies 14 (2021) 2406.
[5] S.A. Bari, M. Fuad, K.F. Labib, M.M. Ehsan, Y. Khan, M.M. Hasan, Enhancement of thermal power plant performance through solar-assisted feed water heaters: an innovative repowering approach, Energy Convers. Management: X (2024) 100550.
[6] S. Zinatloo-Ajabshir, M. Salavati-Niasari, Preparation of magnetically retrievable CoFe2O4@ SiO2@ Dy2Ce2O7 nanocomposites as novel photocatalyst for highly efficient degradation of organic contaminants, Compos. B Eng. 174 (2019) 106930.
[7] S. Zinatloo-Ajabshir, S. Rakhshani, Z. Mehrabadi, M. Farsadrooh, M. Feizi-Dehnayebi, S. Rakhshani, M. Dušek, V. Eigner, S. Rtimi, T.M. Aminabhavi, Novel rod-like [Cu (phen) 2 (OAc)]· PF6 complex for high-performance visible-light-driven photocatalytic degradation of hazardous organic dyes: DFT approach, Hirshfeld and fingerprint plot analysis, J. Environ. Manage. 350 (2024) 119545.
[8] S. Zinatloo-Ajabshir, Z. Salehi, O. Amiri, M. Salavati-Niasari, Green synthesis, characterization and investigation of the electrochemical hydrogen storage properties of Dy2Ce2O7 nanostructures with fig extract, Int. J. Hydrogen Energy 44 (2019) 20110–20120.
[9] M.M. Hossain, M.S. Hossain, N.A. Ahmed, M.M. Ehsan, Numerical Investigation of a modified Kalina cycle system for high-temperature application and genetic algorithm based optimization of the multi-phase expander's inlet condition, Energy and AI 6 (2021) 100117.
[10] M.M. Hossain, N.A. Ahmed, M.A. Shahriyar, M.M. Ehsan, F. Riaz, S. Salehin, C. A. Salman, Analysis and optimization of a modified Kalina cycle system for low-grade heat utilization, Energy Convers. Management: X 12 (2021) 100121.
[11] S. Zinatloo-Ajabshir, M.S. Morassaei, O. Amiri, M. Salavati-Niasari, L.K. Foong, Nd2Sn2O7 nanostructures: green synthesis and characterization using date palm extract, a potential electrochemical hydrogen storage material, Ceram. Int. 46 (2020) 17186–17196.
[12] S. Zinatloo-Ajabshir, M.S. Morassaei, M. Salavati-Niasari, Simple approach for the synthesis of Dy2Sn2O7 nanostructures as a hydrogen storage material from banana juice, J. Clean. Prod. 222 (2019) 103–110.
[13] O.C. Change, Intergovernmental panel on climate change, World Meteorological Organization 52 (2007) 1–43.
[14] R. Stanger, T. Wall, R. Spörl, M. Paneru, S. Grathwohl, M. Weidmann, G. Scheffknecht, D. McDonald, K. Myöhänen, J. Ritvanen, S. Rahiala, T. Hyppänen, J. Mletzko, A. Kather, S. Santos, Oxyfuel combustion for CO2 capture in power plants, Int. J. Greenhouse Gas Control 40 (2015) 55–125.
[15] H. Jericha, W. Saw, E. Göttlich, Design concept for large output Graz Cycle gas turbines, J. Eng. Gas Turbines Power-Trans. Asme 130 (2008).
[16] P. Mathieu, R. Nihart, Zero-emission MATIANT cycle, J. Eng. Gas Turbines Power-Trans. Asme 121 (1999) 116–120.
[17] O. Bolland, P. Mathieu, Comparison of two CO2 removal options in combined cycle power plants, Energ. Conver. Manage. 39 (1998) 1653–1663.
[18] R. Anderson, F. Viteri, R. Hollis, A. Keating, J. Shipper, G. Merrill, C. Schillig, S. Shinde, J. Downs, D. Davies, M. Harris, Oxy-Fuel Gas Turbine, Gas Generator and Reheat Combustor Technology Development and Demonstration, in: ASME Turbo Expo 2010: Power for Land, Sea, and Air, Vol. Volume 3: Controls, Diagnostics and Instrumentation; Cycle Innovations; Marine, 2010, pp. 733-743.
[19] R.J. Allam, M.R. Palmer, G.W. Brown, J. Fetvedt, D. Freed, H. Nomoto, M. Itoh, N. Okita, C. Jones, High efficiency and low cost of electricity generation from fossil fuels while eliminating atmospheric emissions, including carbon dioxide, Ghgt-11 37 (2013) 1135–1149.
[20] L. Mancuso, N. Ferrari, P. Chiesa, E. Martelli, M.J.I.r. Romano, Oxy-combustion turbine power plants, 5 (2015).
[21] S.S. Bishal, D.F. Faysal, M.M. Ehsan, S. Salehin, Performance evaluation of an integrated cooling and power system combining supercritical CO2, gas turbine, absorption refrigeration, and organic rankine cycles for waste energy recuperating system, Results in Engineering 17 (2023) 100943.
[22] S.S. Bishal, A.I. Anando, D.F. Faysal, M.M. Ehsan, Performance evaluation of a novel multigeneration plant of cooling, power, and seawater desalination using supercritical CO2 partial cooling, ME-TVC desalination, and absorption refrigeration cycles, Energy Convers. Manage.: X 20 (2023) 100485.
[23] R. Scaccabarozzi, M. Gatti, E. Martelli, Thermodynamic analysis and numerical optimization of the NET Power oxy-combustion cycle, Appl. Energy 178 (2016) 505–526.
[24] Z.L. Zhu, Y.P. Chen, J.F. Wu, S.B. Zhang, S.X. Zheng, A modified Allam cycle without compressors realizing efficient power generation with peak load shifting and CO2 capture, Energy 174 (2019) 478–487.
[25] E. Dokhaee, A. Saraei, S.J. Mehrabadi, P. Yousefi, Simulation of the Allam cycle with carbon dioxide working fluid and comparison with Brayton cycle, Int. J. Energy Environ. Eng. 12 (2021) 543–550.
[26] W. Chan, X.L. Lei, F.C. Chang, H.X. Li, Thermodynamic analysis and optimization of Allam cycle with a reheating configuration, Energ. Conver. Manage. 224 (2020) 113382.
[27] Y.M. Zhao, B. Wang, J.L. Chi, Y.H. Xiao, Parametric study of a direct-fired supercritical carbon dioxide power cycle coupled to coal gasification process, Energ. Conver. Manage. 156 (2018) 733–745.
[28] T. Xin, C. Xu, Y. Zhang, L. Yu, H. Xu, Y. Yang, Process splitting analysis and thermodynamic optimization of the Allam cycle with turbine cooling and recompression modification, Energy 286 (2024) 129458.
[29] R. Allam, S. Martin, B. Forrest, J. Fetvedt, X.J. Lu, D. Freed, G.W. Brown, T. Sasaki, M. Itoh, J. Manning, Demonstration of the Allam Cycle: An update on the development status of a high efficiency supercritical carbon dioxide power process employing full carbon capture, 13th International Conference on Greenhouse Gas Control Technologies, Ghgt-13, 114 (2017) 5948-5966.
[30] Z. Wang, Y.J.R. Li, S.E. Reviews, Layer pattern thermal design and optimization for multistream plate-fin heat exchangers—a review, 53 (2016) 500-514.
[31] V. Kindra, I. Komarov, S. Osipov, O. Zlyvko, I. Maksimov, Feasibility study of the CO2 regenerator parameters for oxy-fuel combustion power cycle, Inventions 7 (2022) 66.
[32] A. Rogalev, N. Rogalev, V. Kindra, A. Vegera, A. Zonov, Multi-stream heat exchanger for oxy-fuel combustion power cycle, AIP Conference Proceedings Vol. 2323 (2021).
[33] G. Rodríguez Hervás, F.J.E. Petrakopoulou, Fuels, Exergoeconomic analysis of the allam cycle, 33 (2019) 7561-7568.
[34] W. Chan, H.X. Li, X. Li, F.C. Chang, L.L. Wang, Z.M. Feng, Exergoeconomic analysis and optimization of the Allam cycle with liquefied natural gas cold exergy utilization, Energ. Conver. Manage. 235 (2021) 113972.
[35] D. Fernandes, S. Wang, Q. Xu, R. Buss, D.I. Chen, Process and Carbon Footprint Analyses of the Allam Cycle Power Plant Integrated with an Air Separation Unit, Clean Technologies 1 (2019) 22.
[36] B. Linnhoff, J.R. Flower, Synthesis of heat exchanger networks: I. Systematic generation of energy optimal networks, AIChE Journal 24 (2004) 633–642.
[37] W. Chan, T. Morosuk, X. Li, H.X. Li, Allam cycle: review of research and development, Energ. Conver. Manage. 294 (2023) 117607.
[38] C.W. White, N.T. Weiland, Evaluation of property methods for modeling direct-supercritical CO2 power cycles, J. Eng. Gas Turbines Power-Trans. Asme 140 (2018) 011701.
[39] D. Fiaschi, G. Manfrida, P. Mathieu, D. Tempesti, Performance of an oxy-fuel combustion CO2 power cycle including blade cooling, Energy 34 (2009) 2240–2247.
[40] S. Yadav, S.J.F. Mondal, A review on the progress and prospects of oxy-fuel carbon capture and sequestration (CCS) technology, 308 (2022) 122057.
[41] S. Hume, Performance evaluation of a supercritical CO2 power cycle coal gasification plant, in: Proc. 5th Int. Symp. of Supercritical CO2 Power Cycles, San Antonio, 2016.
[42] N. Weiland, W. Shelton, C. White, D. Gray, Performance baseline for direct-fired sCO2 cycles, in: Proc. 5th Int. Symp. of Supercritical CO2 Power Cycles, San Antonio, 2016.
[43] G. Beysel, Enhanced Cryogenic Air Separation. A proven Process applied to Oxyfuel. Future Prospects, in: 1st Oxyfuel Combustion Conference, Cottbus, Germany, Vol. 8, 2009.
[44] J. Luo, O. Emelogu, T. Morosuk, G. Tsatsaronis, Exergy-based investigation of a coal-fired allam cycle, Energy 218 (2021) 119471.
[45] F. Yilmaz, M. Ozturk, R. Selbas, Design and thermodynamic analysis of coal-gasification assisted multigeneration system with hydrogen production and liquefaction, Energ. Conver. Manage. 186 (2019) 229–240.
[46] M.R. Gómez, R.F. Garcia, J.R. Gómez, J.C. Carril, Thermodynamic analysis of a Brayton cycle and Rankine cycle arranged in series exploiting the cold exergy of LNG (liquefied natural gas), Energy 66 (2014) 927–937.
[47] Y. Wu, Z. Wang, Y. Liu, Q. Guo, Z. Wen, D. Chen, K. Gong, P. Zhu, G. Xiao, Performance analysis of a modified Allam cycle combined with an improved LNG cold energy utilization method, J. Renew. Sustain. Energy 16 (2024).
[48] J.-Q. Guo, M.-J. Li, J.-L. Xu, J.-J. Yan, T. Ma, Energy, exergy and economic (3E) evaluation and conceptual design of the 1000 MW coal-fired power plants integrated with S-CO2 Brayton cycles, Energ. Conver. Manage. 211 (2020) 112713.
[49] Z. Guo-Yan, W. En, T. Shan-Tung, Techno-economic study on compact heat exchangers, Int. J. Energy Res. 32 (2008) 1119–1127.
[50] S. Saqline, L. Yang, A. Romagnoli, W.J.J.o.C.P. Liu, Coupling chemical looping air separation with the Allam cycle–A thermodynamic analysis, 418 (2023) 138097.